Combustion and Flame 197 (2018) 340–354

Contents lists available at ScienceDirect

Combustion and Flame

journal homepage: www.elsevier.com/locate/combustflame

Scaling nonreactive cross flow over a heated plate to simulate forest fires

Nikolay Gustenyov[a], Nelson K Akafuah[a], Ahmad Salaimeh[a], Mark Finney[b], Sara McAllister[b], Kozo Saito[a,*]

[a] Department of Mechanical Engineering, IR4TD, University of Kentucky, 151 RGAN, Lexington, KY 40506-0503, USA
[b] USDA Forest Fire Science Laboratory, Missoula, MT, USA

ARTICLE INFO

Article history:
Received 24 May 2018
Revised 29 June 2018
Accepted 22 August 2018
Available online 7 September 2018

Keywords:
Forest fire
Flow visualization
Scaling laws
Wind tunnel convective flow experiments

ABSTRACT

The paper reports visualization of the flow of smoke over a flat surface inside of a low-speed wind tunnel. A heating plate flush mounted on the wind tunnel floor simulated a spreading line fire that produces uniform heat flux under constant wind speed condition. A paper-thin cloth was soaked with commercially available Vaseline and placed on top of the heating plate; when it is heated, it produced thick white smoke, ideal for flow visualization. Two sides and top of the wind tunnel were made of a transparent acrylic sheet that enabled LED and laser sheet light illumination of the flow. A still camera with a full-frame CMOS sensor was used to record time-series images of illuminated smoke flow patterns from different angles. From these images, the following four flow structures were identified: organized horizontal vortex flows, weak vortex flow interactions, strong vortex flow interactions (also described as the 'transition regime'), and, turbulent flows. Previously developed scaling laws on forest fires were applied to find similarity in flow structures created by the current small-scale convective heat-transfer experiments and the USDA's mid-scale wind tunnel fire experiments.

1. Introduction

Wildland fires have been studied extensively through experimental testing and mathematical modeling to understand their behavior relative to predicting their behavior for known fuel properties, heat and moisture contents. Wildland fires spread over a wide variety of fuels, and the weather patterns and conditions can change dramatically during it, thereby diminishing the predictive capabilities of models.

Many current models attempt to explain full-scale observations that correlate fire spread rates with the fuel type and weather conditions without sufficient considerations of the physics governing fire spread and intensities. Byram [1] and Byram et al. [2] provided a historically important framework for modeling of free burning fires, stressing that a successful model requires understanding of the basic physical mechanisms of fire spread and to uncertainty as to the relative significance of the many variables that enter the problem of fire spread. Byram et al. [2] designed laboratory scale wood crib fires and found that both slope and wind speed had minor effects on the burning rate of the fuel bed. Interestingly, their findings support scaling laws on pool and crib fires [3] which we applied as the base to support the current flow visualization experiments. Recently Nelson [4] further developed Byram's original criteria of the ratio of power of fire to the power of inertial force for forest fires to more general large-scale phenomena where both buoyancy and inertial forces interact. Following the Byram's principles, we conducted this study to investigate the fundamental physics that govern laboratory and mid-scale tests with an eye on improving our understandings of wildland fire behaviors [5].

There is rich literature in forest fire research and it is not possible to reference all the published articles here. We only selected notable studies that have a high impact to our current study.

Fuel ignitability is crucial for initiating and sustaining wildfires [6] that are started through either spontaneous or piloted ignition. Spontaneous ignition occurs without interactions between an external pilot flame and unburnt fuel; this type of ignition requires intense heat flux to sustain burning and therefore is rare. In contrast, piloted ignition is the dominant mechanism due to the presence of radiative and convective heating of unburnt fuel plus the influence of an open flame [7].

The mechanism of forest fire spread have been explored for at least seventy years, searching for the role of radiation and convection over different types of forest fuel beds, weather and environmental conditions. The role of convective heat transfer on the fire spread was investigated by laboratory-scale experiments

* Corresponding author.
E-mail addresses: ksaito@uky.edu, saito@engr.uky.edu (K. Saito).

https://doi.org/10.1016/j.combustflame.2018.08.014
0010-2180/

Nomenclature

c_p	specific heat of the gas at atmospheric pressure (kJ/kg K)
c_2	specific heat of fuel (kJ/kg K)
E	irradiance received by radiometer (kJ/K m^2)
g	gravitational acceleration (m/s^2)
I	fire intensity (kJ/m s)
q_f	heat value per unit mass of fuel (kJ/kg)
T	heater surface temperature (K)
t	characteristic time (s)
$\Delta\theta_1$	temperature change of air and gas (K)
$\Delta\theta_2$	temperature change of fuel (K)
λ	latent heat per unit mass of fuel (kJ/kg)
$\emptyset$	the ratio of consumed fuel to the total fuel available (dimensionless)
u	horizontal wind velocity (m/s)
L_w	depth of the flame zone where combustion takes place (m)
L_f	average flame height (m)
L_a	average plume height (m)
ρ_1	the density of hot gases in the plumes (kg/m^3)
ρ_2	the density of unburnt fuel (kg/m^3)
H	height of the discrete fuel particles or fuelbed (m)
L_e	preheating length, defined as distance ahead of the flame where unburnt fuel experiences significant heat transfer from the flame (m)
W	the characteristic frequency that represents a time dependent behavior/instability such as vortex shedding (s^{-1})
Γ	geometrical similarity (dimensionless)
l_2	the characteristic length that represents distance between two valleys or width of a flame tower or wavelength within a fire front (m).

[8–11] and by both analytical and mathematical modeling [12–15]. As to the role of radiation, Albini [16] and Telisin [17] suggested that intense radiation from the flame front contributed to fuel preheating and fire spread. Subsequently, Butler et al. [18] indicated that convective cooling could be significant before ignition and that convective heating immediately before and at the time of ignition is extreme in typical wildland fires. Emori et al. [19], by studying flame spread through horizontal and inclined fuel beds made of excelsior and vertically oriented paper strips coated with candle wax, showed that convection governed flame spread in these cases. Emori and Saito [3] also characterized in their scaling laws how the spread of convective-driven fires was different from the spread of radiative-driven fires. Pool fires, for whose diameter is larger than 1 m, are driven by radiation whereas convection drives wood crib fires; these differences have to be considered in the governing mechanisms of flame propagation [20].

Finney et al. [5] and Adam et al. [21] further developed the idea that convective heat transfer before ignition by either direct flame impingement or natural convective heating circulation played a more substantial role in wildland fire spread than previously believed. They conducted laboratory ignition tests [22] on live pine samples that were heated by either radiation or convection. They found that pine needle samples will not ignite solely from radiation even at an extreme level of pre-ignition flux of 80 kW/m^2 for more than 10 min [22,23]. In comparison, the same live pine samples exposed to the convective heating flux of 25 kW/m^2 ignited in less than 10 s. Based on this and other similar repeated test results, they concluded: “Convective cooling of the fine-sized fuel particles in wildland vegetation is observed to offset efficient heating by thermal radiation until convective heating by contact with flames and hot gasses occurs” [22]. It was also pointed out that including convection in models is considerably different than isolating its role in particle ignition and wildfire spread, and that requirements for particle ignition by radiation and convection vary with particle size [5,21,22].

Finney et al. [5] and Emori et al. [24] stated that wildfires are intrinsically dynamic, but the causes and mechanisms of their dynamic nature have not yet been well investigated. The dynamic interactions between the flame, fuel and the gas flow field instill difficulties in wildfire research that may not be present in other types of fires [25]. Unsteady flame behaviors, such as flickering, pulsing and vortex shedding that are caused by the interaction between the diffusion flame (including forest fires) and gas flow have been observed many times in wildfires [26–31]. The presence of wind has a critical effect on wildland fire behavior – it causes time-dependent vortex shedding which improves convective heat transfer [32–34]. Therefore, the study of convective heat transfer from a static, or time-averaged, perspective cannot address important questions and, as a result, could prevent accurate predictions of wildfire behaviors. A series of elaborate PIV studies [35–37] revealed vortices in the preheating gas phase region of spreading fires. The reference [37] showed that there were three different-size vortices, 40, 30, and 20 mm, and each played a different role at the progressing flame front. The 40-mm-vortex pushed by the propagating flame to the flame front and slowly consumed the trapped fuel, the 30-mm-vortex allowed the flame to propagate around it and then rapidly consumed the vortex, and the fire rapidly consumed the 20-mm-vortex. The identified small vortices may trap premixed fuel-air mixture and become a flame precursor to spread fire front, which may deserve further study.

A series of wind tunnel, fire spread experiments using engineered cardboard fuelbeds have been conducted [22]. Two dynamic features were identified within the flame zones: convective flame peaks and valleys separated by regular spacings that moved back-and-forth in a span-wise direction; and, the number of peaks depended on the fuel properties and fuelbed geometry. The same type of behavior was observed in the progressing front of a wildfire when the flame split into peaks [22,38]. This behavior is of paramount interest because it has been examined very little, even though most previous laboratory fire studies have used well-defined fuels under controlled environments with, possibly, the application of scaling laws [38].

The historically significant past studies by Scesa [12] and Anderson [14] demonstrated that forest fires and their spreading mechanism can be described by the mass, momentum and energy balance, when the fast rate chemical reaction is assumed to produce the fire generated heat which becomes the source of heating unburned fuel located in the downstream. These past studies, as well as scaling law studies [3,39] suggest that the fire generated heat can be simulated by the use of an alternative non-combustion heat source to satisfy the proposed governing equations [12,14] and scaling laws [3,39]. Emori and Saito [40] developed an experimental technique to use the heated nichrome wire to simulate the spreading line fire. Later Haines and Smith [41–43] applied the heated wire method to successfully produce vortex pairs and collapse during wildland fires using small-scale wind tunnel flow visualization experiments.

Hence, this work focuses on fluid dynamic aspects of flow behavior expected for fires by replacing the chemical reactions of fire by an electrical heater as the thermal energy source. Elimination of flame significantly simplifies the study of fire dynamics and permits visualization of flow fields, usually masked by flames. In addition, to assess similarities between a mid-scale wind tunnel fire and the current electric heater-generated flow-field, scaling analysis was conducted. Use of this heater provided more

precise temperature control, made easier the investigation of buoyancy forces, and enabled scaling laws to be applied with rather-controlled, variable temperatures and heat fluxes. We investigated the time-dependent nature of fire behavior and the role of convection heat transfer in fire spread, whether convective heat transfer is effective in fire spread for limited distances ahead of a fire front.

It must be mentioned that Haines [44] and Haines and Smith [41–43] applied low speed airflow parallel to the heated wire which represents fire generated heat, the technique originally developed by Emori and Saito [40] to reconstruct a moving fire whirl to investigate the 1978 Mt. Nuke fire accident which caused several firefighters' deaths. They succeeded in recreating vortex pairs above the wire and suggested Gr number and Ra number for scaling without specifically validating the role of each of these pi-numbers, to help connect their laboratory observations to the full-scale fires. To appreciate their pioneer studies, we applied our scaling laws [3] to design the current flow visualization experiments, where we clarified assumptions and physical meaning of pi-numbers (dimensionless number). Despite the different flow orientation relative to the heater between Haines and Smith [41–43] and the current study, both studies found very similar shape vortices, indicating that Haines and Smith's horizontal vortices might well be formed in the current experiments, which is a scaled-down version of the USDA's fire spreading experiments [22]. This seemingly coincidental finding suggests the need for further study whether or not the horizontal vortices and the USDA's convection-driven fire spreading model [22] is related each other.

2. Scale modeling

There are a variety of studies from fundamental curiosity-driven research that seek primary control mechanisms within laboratory-scale fires (e.g., Williams [45]) to studies that seek scaling laws to establish correlations between laboratory experiments and full-scale wildfires. This paper focuses on the latter aspects; the following provides a brief review of previous scaling studies.

Hottel [20] addressed radiation in fire modeling and reframed previous experimental results. Spalding [46] and Williams [39] both over-constrained their scaling laws and found that the quantity of Pi-numbers to be obeyed far exceeded the number of degrees of freedom. Consequently, they proposed relaxation or partial modeling to obtain a result [47], but did not introduce a systematic method for evaluating relaxation. Emmons [48,49] focused on liquid pool fires and paper arrays, paving the way for Emori and Saito [3] to differentiate radiation-dominated combustion in pool fires from the convection-driven combustion in crib fires. Using the law approach [24], Emori and Saito identified seventeen Pi-numbers that described the scaling in both types of fires and reduced these to five by use of a systematic relaxation technique [3]; these five Pi-numbers were validated in scale model experiments [3]. Their scaling laws also extended into flame spread [19] while using excelsior fuel beds and paraffin coated paper strip fuel beds; the latter was similar to the engineered cardboard structure more recently adopted by the USDA [5,21]. Note that Pagni and Peterson [15] conducted a qualitative analysis of one-D steady-state propagation on porous fuel beds including ambient wind, fuel moisture content, fuel bed slope, and fuel pyrolysis. They found that for no wind condition, radiation from flame mainly controlled the flame spread with minor contribution from the glowing embers and conduction; their findings match to scaling laws on pool fires [3]. For wind-aided fire spreading, convection heat transfer becomes dominant, while flame radiation may provide the significant portion of heating depending on the extent of wind, agreement with scaling laws on crib fires [3] and spreading fires [19]. Pagni and Peterson's [15] dimensionless groups basically share the same pi-number groups of [3], which were obtained by combination of dimensional analysis and the law approach by identifying governing physics, which overlaps with [15].

The current study focuses on fluid dynamics aspect of fire behavior using visualization as a primary tool. Small-scale laboratory experiments were designed and performed to study interactions between buoyant and inertia forces without the presence of flames because the presence of flames can mask these interactions; then, similarities between the small-scale results and the USDA's wind tunnel fire spread experimental results were assessed by conducting a scaling analysis.

This study employed the following assumptions.

1. Air and gas flow within and around flames are turbulent [19,50,51]. This situation means that inertial and buoyant forces dominate over viscous force. This assumption is supported by data and discussions from previous studies which classified flow fields within crown [52,53], grass [54], crib [3,55] and wind tunnel fires [56,57] as turbulent.
2. Convection drives heat transfer from the flame to the unburnt fuel. The dominant heat transfer mode in large grass fires, crib fires, and wind tunnel experiments is convective [3,58,59,60].
3. Fire propagates along a horizontal surface with the horizontal wind in the direction of fire spread, i.e., fire spread in only a single direction.
4. Wind tunnel provides a well-regulated constant and steady horizontal airflow.
5. The vertical (upward) component of flow velocity is due to buoyancy.
6. The fuelbeds were considered continuous and uniform and consist of discrete fuel particles with known fuel and thermal physical properties. This assumption would satisfy the identical fuel property condition in selecting Pi-numbers for scale-model fire experiments. Heat flux in the present model simulates the heat generated by the flame.

The following seven physical parameters and equations, including two forces and five heats, were considered significant for performing the scaling analysis. Note that geometrical similarity represented by Γ, which can include the inclination of plume by wind effect is automatically included to the scaling requirements based on scale modeling theory [24,47]. See Fig. 1 for dimensions.

- $F_i = \rho_1 l_2 L_a u^2 =$ inertial force of air and gas;
- $F_b = \Delta\rho_1 l_2 L_w L_a g =$ buoyant force of air and gas;
- $Q = \emptyset q_f \rho_2 l_2 H L_w = I L_w t =$ heat generated;
- $Q_r = E l_2 L_e t =$ radiant heat received by unburnt fuel;
- $Q_{c1} = c_p \rho_1 L_a l_2 L_e \Delta\Theta_1 =$ heat stored in air and gas associated with temperature rise;
- $Q_{c2} = c_2 \rho_2 l_2 H L_e \Delta\Theta_2 =$ heat stored in unburnt fuel;
- $Q_\lambda = \lambda \rho_2 l_2 H L_e =$ latent heat of fuel.

Using the law approach [24] and these aforelisted equations, the following six independent Pi-numbers were identified [19]:

$$\pi_1 = \frac{F_i}{F_b} = \frac{\rho_1 u^2}{\Delta\rho_1 L_w g} = Froude\ number$$

$$\pi_2 = \frac{Q_r}{Q} = \frac{E l_2 L_e}{I L_w}$$

$$\pi_3 = \frac{Q_{c1}}{Q} = \frac{c_p \rho_1 l_2 L_a R \Delta\theta_1}{I L_w}$$

$$\pi_4 = \frac{Q_{c2}}{Q} = \frac{L_e}{L_w}$$

$$\pi_5 = \frac{Q_\lambda}{Q} = \frac{\lambda L_e}{\emptyset q_f L_w}$$

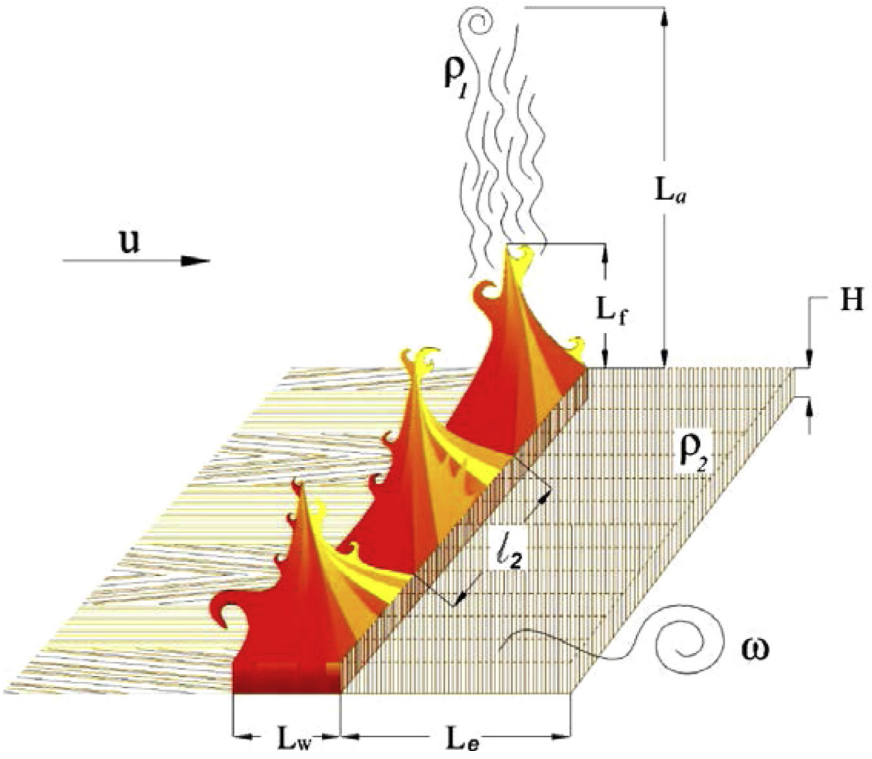

Fig. 1. Schematic of flame spread over a fuelbed [24].

$$\pi_6 = \frac{F_i u t}{Q} = \frac{\rho_1 l_2 L_a u^3}{I L_w}$$

where: $R = Le/t$ = fire spreading rate in the horizontal direction, and $I = \emptyset q_f \rho_2 l_2 H/t$ = fire intensity.

Recently, Finney et al. [22] and Saito and Akafuah [56] found that a Froude (Fr)–Strouhal (St) correlation existed among full-scale crown fires, control burns over grassland, large-scale crib fires and wind tunnel burns of engineered cardboard. This Fr-St correlation was based on the dominance in the upstream fire zone of both external wind and fire-induced flow governed by inertia forces where the interactions between the buoyant and inertial forces caused flame instabilities with a repeating pattern leading to the formation of Gortler vortices in the downstream direction [22]. Hence, the inertial forces upstream ($F_{i,up}$) and downstream ($F_{i,down}$) of a fire zone need to be considered separately. This separation necessitates the use of a seventh Pi-number which is the Strouhal number [19,56] consisting of the ratio between the inertial force causing vortex shedding downstream and the inertial force of airflow upstream of the flames:

$$\pi_7 = \frac{F_{i,down}}{F_{i,up}} = \frac{L_e w}{u} = Strouhal\ number,$$

where w = the downstream pulsing frequency.

Strict scaling criteria [24] demand that all the above seven Pi-numbers remain the same among different scale models but, unfortunately, this requirement often leads to impractical scaling laws [24,39]. Hence, we attempt to achieve partial scaling [24] by introducing the following considerations.

- π_2 can be ignored for non-reactive flow experiments, i.e., no flame, because of the much lower gas temperatures in the scale model experiments as compared to the case when the flame is present and flame spreading occurs [6].
- π_4 is not applicable to non-reactive flow experiments; a constant heater width L_w was used for the present experiments.
- π_5 can be ignored because it includes a fuel dependence (Ø) which was not studied.
- π_6 can be neglected because the u^3 term would have caused very high wind velocities for the scale model and would have changed the nature of the phenomenon, i.e., low wind velocity, under investigation.

As a result, the following three Pi-numbers remained.

$$\pi_1 = \frac{F_{i,up}}{F_b} = \frac{\rho_1 u^2}{\Delta\rho_1 L_w g} = Froude\ number$$

$$\pi_3 = \frac{Q_{c1}}{Q} = \frac{c_p \rho_1 l_2 L_a R \Delta\theta_1}{I L_w}$$

$$\pi_7 = \frac{F_{i,down}}{F_{i,up}} = \frac{L_e w}{u} = Strouhal\ number$$

The scaling criteria [24,56] demand that each of these three Pi-numbers must remain the same between full scale and model, i.e., $\pi_1 = \pi_1$', $\pi_3 = \pi_3$', and $\pi_7 = \pi_7$', where non-prime pi-numbers are for the full scale, and primed pi-numbers are for the corresponding scale model.

3. Experimental methods

A low-speed wind tunnel was constructed with a test section made of transparent acrylic glass (Fig. 2). A digital camera, Canon EOS 5D Mark II with Canon EF 50 mm f/1.8 lens, was used to acquire images. An electrical heating element (1.5 kW) coupled with a temperature feedback controller was used to generate buoyancy-driven upward airflow. After several unsuccessful attempts to visualize this low-speed flow, we finally found that when a paper towel strip soaked in Vaseline was heated above 200 °C, it can produce dense white smoke, ideal for our flow visualization.

To ensure uniform velocity across the test section of the small wind tunnel, two double mesh sheets having 2 mm by 2 mm holes

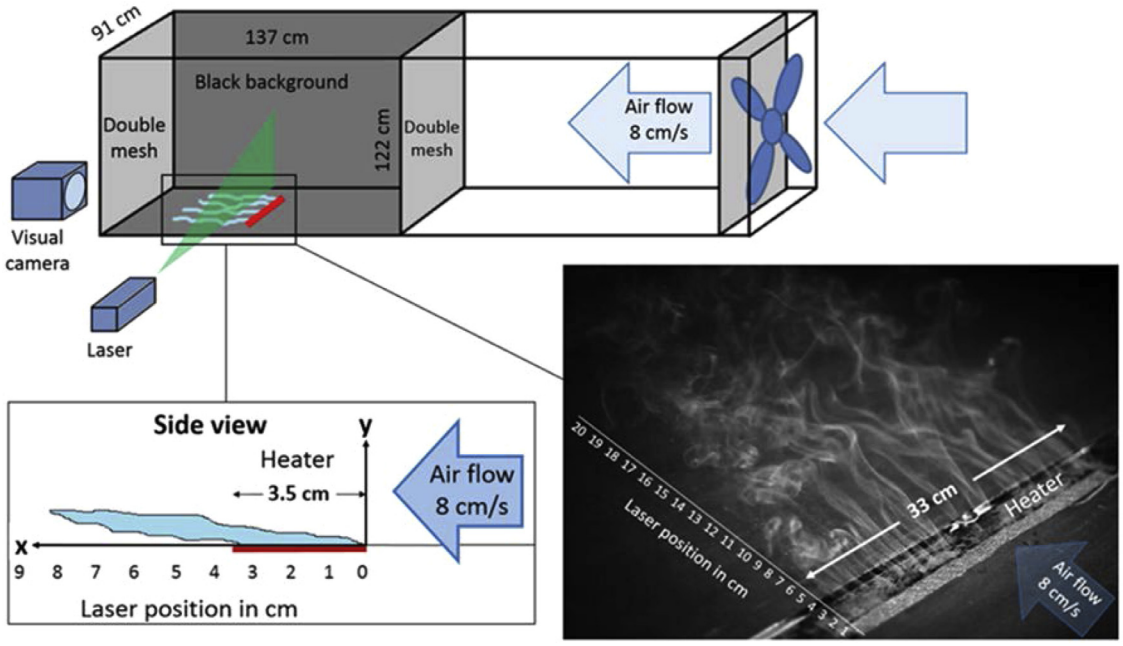

Fig. 2. Flow visualization experimental setup consisting of a low-speed wind tunnel, a heater, a digital camera, a laser and a LED light. Also shown is an image of smoke flowing through the visualization section, illuminated using the LED. (For interpretation of the references to color in this figure, the reader is referred to the web version of this article.)

were placed between the fan and the test section, and one was positioned downstream of the test section. Both the back and bottom sides of the test section were painted in lusterless black to reduce any light reflection and increase the contrast between the illuminated white smoke and black background.

A heater with a surface area of 3.5 cm by 33 cm was mounted perpendicular to horizontal airflow, flush with the bottom surface of the test section. The bottom and sides of the heater were insulated using cement board to ensure the bottom of the test section remained to the ambient temperature even though the heater's top surface was much hotter. The temperature controller allowed precisely-controlled, steady-state temperatures on the top surface of the heater which were measured via a thermocouple placed on the heater under a constant heat flux condition. The heater's dimensions were much smaller than the width of the test section and, with the heater placed symmetrically in the middle of it, little-to-no side wall effects were observed on the main flow of the smoke.

After a paper strip soaked with Vaseline was placed on the heater's surface, the heater controller was set to a temperature of interest, and then the heater was turned on. Once the heater's top surface achieved the desired temperature, a thick, dense white smoke streak arose. The smoke streaks were also illuminated using a compact LED light (60 W) placed inside the test section and mounted on its top side at different locations depending on the angle of image acquisition; the LED within the test section did not affect the airflow. Under the LED illumination, a complex 3D flow structure emerged. To understand this 3D structure, we created a thin laser sheet to dissect it layer by layer.

The laser was solid state, diode-pumped and produced a wavelength of 532 nm (green) with a power of 300 mW; the laser beam was coupled to a cylindrical lens that formed a 2 mm thick laser sheet with an opening angle of 30°. The laser was placed in front of the test chamber (Fig. 2), and the light sheet orientation was parallel to the heater edge and perpendicular the test section floor and air flow direction. The position of illumination from the laser sheet was changed by one-centimeter increments from the front (upstream) edge of the heater to 30 cm downstream from that point. The visual camera was mounted downstream of the test section to capture images of the flow approaching the camera. The camera and the laser illuminated sheet were moved simultaneously to maintain the relative distance between them constant.

A series of preliminary tests showed that 200 °C was the minimum temperature of the heater's surface which gave smoke streaks dense enough for visualization and imaging. Visualization experiments were performed using heater temperatures between 200–500 °C with no horizontal airflow and with airflow. At 200 °C, smoke generation was stable for approximately 20 min while at 300 °C it dropped to about 3 min; ignition of the Vaseline-soaked paper occurred when temperatures exceeded 400 °C. Because establishing an appropriate camera focus setting took up to a few minutes and was the main difficulty at the beginning of each test for imaging the smoke flows, we decided to use a constant temperature of 200 °C for all imaging tests involving external horizontal flow.

The horizontal airflow generated by the fan enabled three controlled velocities of 8, 11 and 15 cm/s (± 15%). These were chosen based on the preliminary experiments which showed that the 8 cm/s flow velocity was the lowest possible for the setup while velocities above 15 cm/s caused erratic flow behaviors that were unsuitable for flow visualization. The flow velocities were measured inside the test section at heights between 1.5 and 30 cm above the floor of the wind tunnel. Smoke streaks, generated outside the test section, were tracked through the test section when the heater was turned off to ensure uniformity and steadiness.

At 200 °C, the convective heat flux from the heater surface, estimated based upon a boundary layer thickness, was 2.0 ± 0.3 kW/m^2; this value was flow velocity dependent. Parameters used for scaling calculations included: L_w (fire zone depth, taken as the heater width = 3.5 cm); L_f (the flame height); and L_e (the preheating length). The values of both L_f and L_e were measured with an IR camera, which was used for our previous heat transfer study [43]; both represented a region where temperatures were significantly above ambient.

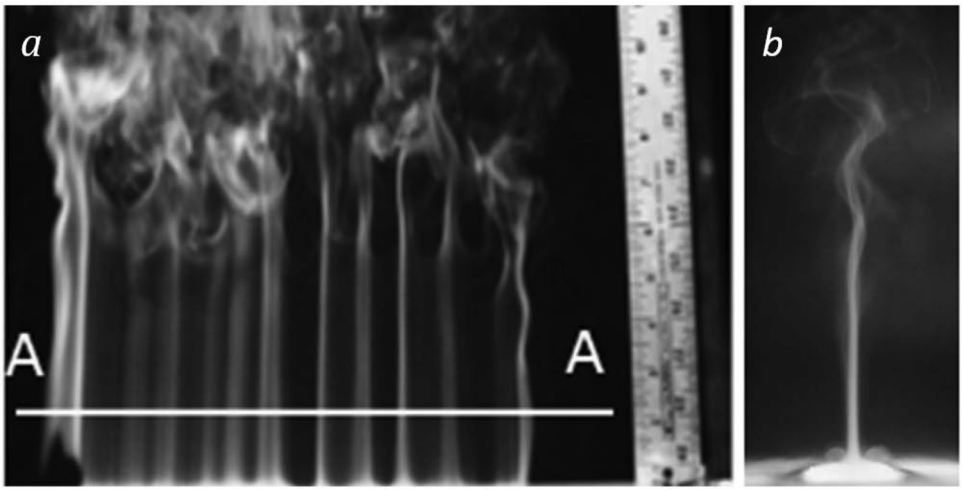

Fig. 3. Smoke streaks arising from the heated surface under no horizontal flow under $T = 400$ °C: front view (a) and side view (b). The cross-section A-A is schematically shown at Fig. 4.

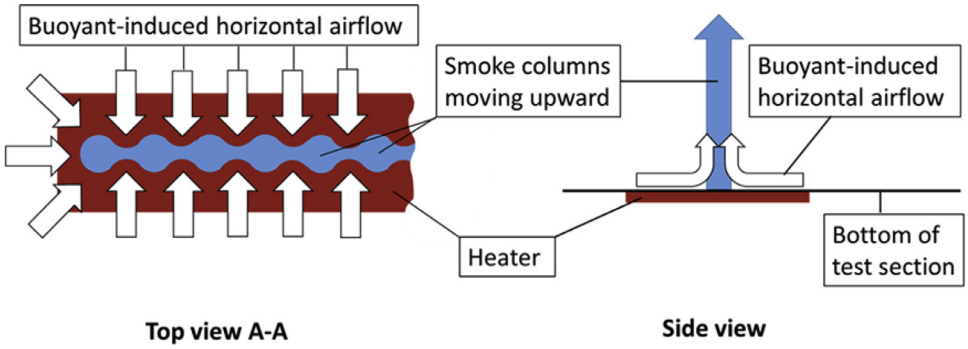

Fig. 4. Schematic diagram of buoyant-induced vertical flow.

4. Results and discussion

The first step was visualization of buoyant driven upward flow with no horizontal flow. The images of smoke flow (Fig. 3) during these tests showed in detail the upward flow structure of smoke arising from the heated Vaseline soaked paper.

The rising smoke formed discrete vertical columns organized along the length of heater surface, and the locations of these columns remained the same during each test. Additionally, as seen in the side view image in Fig. 3a, the smoke columns emanated along and from the total length of the heater. They were rising laminar upward flow (Fig.4). After they traveled a certain distance, they evolved into turbulent flow. As the temperature of the heater was increased, the number of columns (Fig. 5) decreased, and their diameters increased. Figure 5 also shows that the average distance at which turbulent flow was established above the heater became smaller with an increase in the heater temperature; the error bars in Fig. 5 represent the minimum and maximum measured values. The intensity of fluctuations in the upward laminar flow increased with an increase in temperature. The same trend was observed in variations of the number of columns: at higher temperatures, the variation in the number of columns increased because of larger heat flux that may have created additional energy to split the flow into columns.

The second step was to capture images of the dynamic interaction between the buoyant-induced upward flow and the horizontal airflow. Smoke streaks generated by the Vaseline-soaked paper on the heater were carried horizontally by the airflow from the wind tunnel whose behavior was illuminated by the LED light and the laser sheet, as explained previously. Imaging was accomplished from four different view angles, shown in Fig. 6a–d, where the discrete smoke streaks are moving downstream at a small upward angle relative to the horizontal direction.

The 2D laser sheet illumination and imaging showed that the structures of the individual smoke streaks were vortex tubes which always appeared in pairs with opposite directions of rotation, as shown in Fig. 7.

A 3.5 cm wide paper strip soaked with Vaseline covered the entire surface of the heater to produce the side view images shown in Fig. 6c and d. They showed the vortex tubes occasionally formed multiple-level structures where tubes originating close to the upstream edge of the heater were generally higher above the wind tunnel floor than tubes formed closer to tail edge of the heater.

This observation initiated further investigations by using narrower Vaseline-soaked paper strips to capture the evolution of single-level smoke flow structure consisting of discrete vortex tubes at a fixed height. We placed a 1 cm width paper strip at three different locations along the x-coordinate and found the flow structure stayed the same regardless of the width of the paper strip.

Figure 8 shows that the smoke streak behavior was similar for $u = 8$, 11 and 15 cm/s under $T = 200$ °C.

We saw that smoke vortex tubes formed over the heater surface flowed downstream independently, and then at a certain distance, they interacted with each other to produce turbulent flow. With the higher wind tunnel generated horizontal airflow, the location of this transition point along the x-coordinate shifted

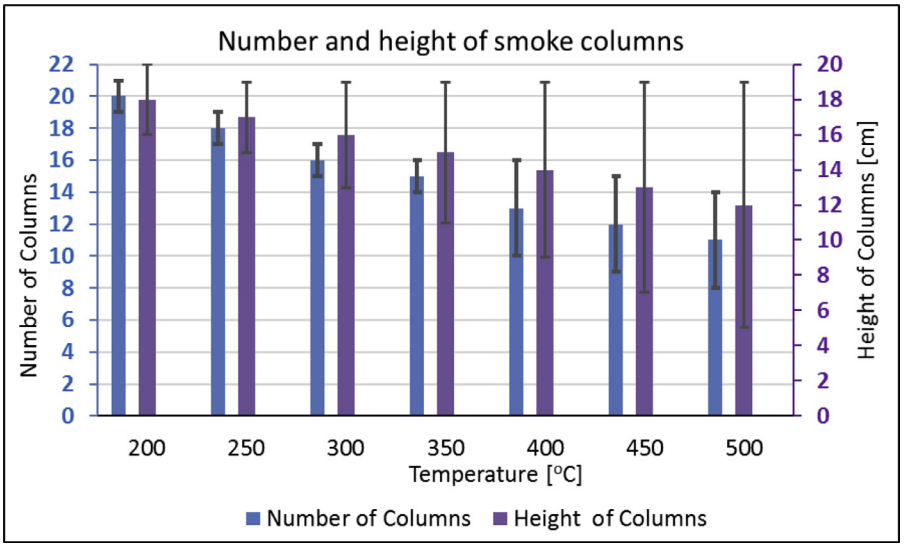

Fig. 5. Number and height of smoke columns depending on the temperature of the heater.

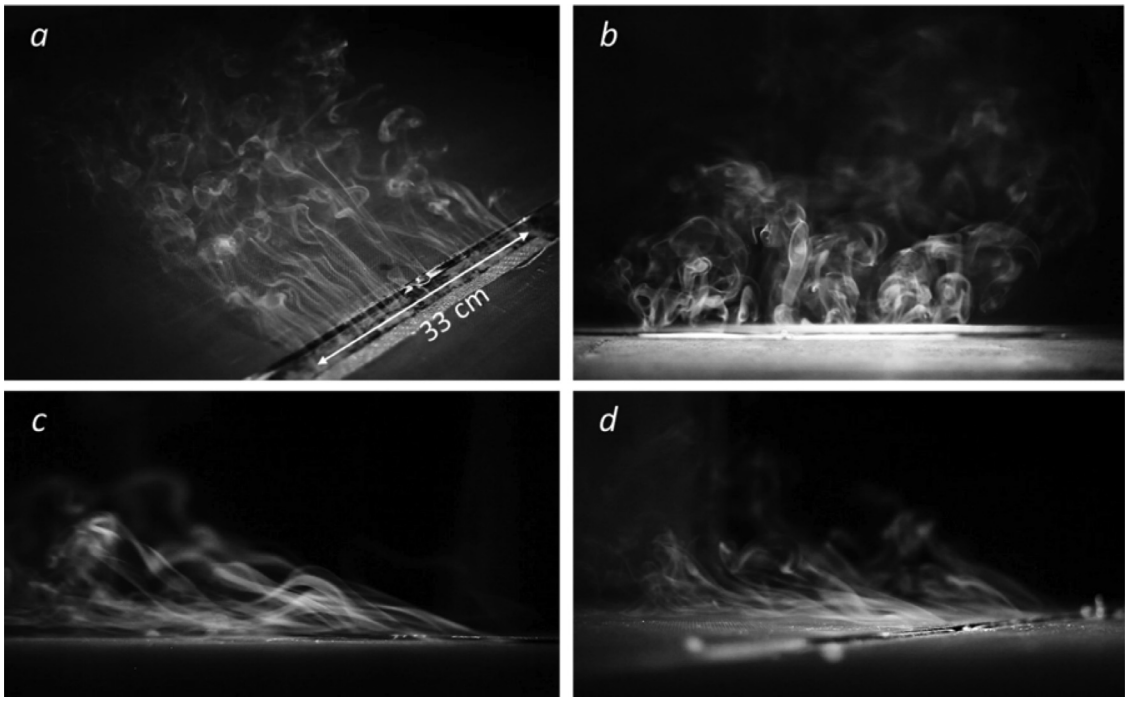

Fig. 6. Flow visualization using LED light at 200 °C; a – top view, b – front view of approaching flow, c – side view downstream of the heater and d – side view upstream of the heater.

toward the downstream and at the lower height in the *y*-coordinate. Figure 8 shows that at $u = 15$ cm/s, the discrete vortices were well-organized and remained intact for greater distances than the lower velocity cases, $u = 8$ and 11 cm/s. That is because the stronger inertial force under the higher horizontal airflow velocity overcame the upward buoyancy force for a longer x distance at a lower y height. Figure 9 summarizes the above trend in the minimum, average and maximum values for the x-length and y-height of the vortices. At the horizontal air velocity of 8 cm/s, the well-organized vortex region remained until $x = 14$ cm, then for $x > 14$ cm, the flow transitioned into turbulent flow. Another interesting observation is: the flow height y drastically increased at $x = 0$–5 cm where the vortices were formed, and between 14 and 18 cm where the transition to turbulent flow occurred; flow directions were almost horizontal between x distances of 5–14 cm.

An airflow velocity of 11 cm/s shifted the turbulent transition region to $x = 16$–20 cm; with the airflow velocity = 15 cm/s, the turbulent transition region occurred at $x = 19$–25 cm.

Figure 10 shows the smoke streak structure taken from both front and side under $u = 8$ cm/s, and the variations in the height of vortices. The smoke streaks on the left side are closer to the floor than the right side images. The circled areas in Fig.s 10–12 show mushroom shape twin vortices; a similar type of twin vortices are often observed at a horizontal distance x close to and within the turbulent transition region. The twin vortices occasionally appeared at smaller x distances were thought to be a significant contributor to variations in smoke flow height as represented by the upper range of the dotted lines in Fig. 9.

Hence, variations in the length of vortex tubes were usually a consequence of the upward motion within the mushroom shape

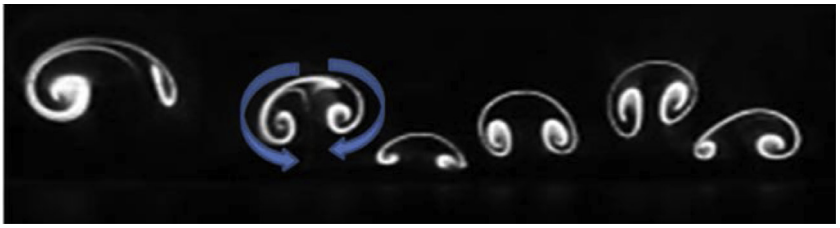

Fig. 7. Vortex pairs at $x = 8$ cm (laser illumination).

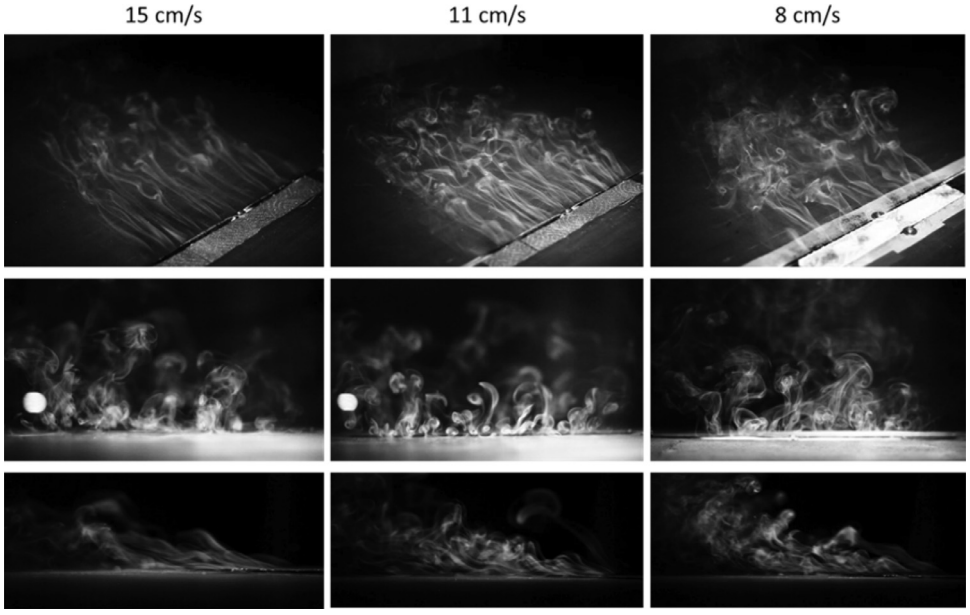

Fig. 8. Visualization of smoke streaks' behavior for $u = 8$, 11, and 15 cm/s under $T = 200$ °C.

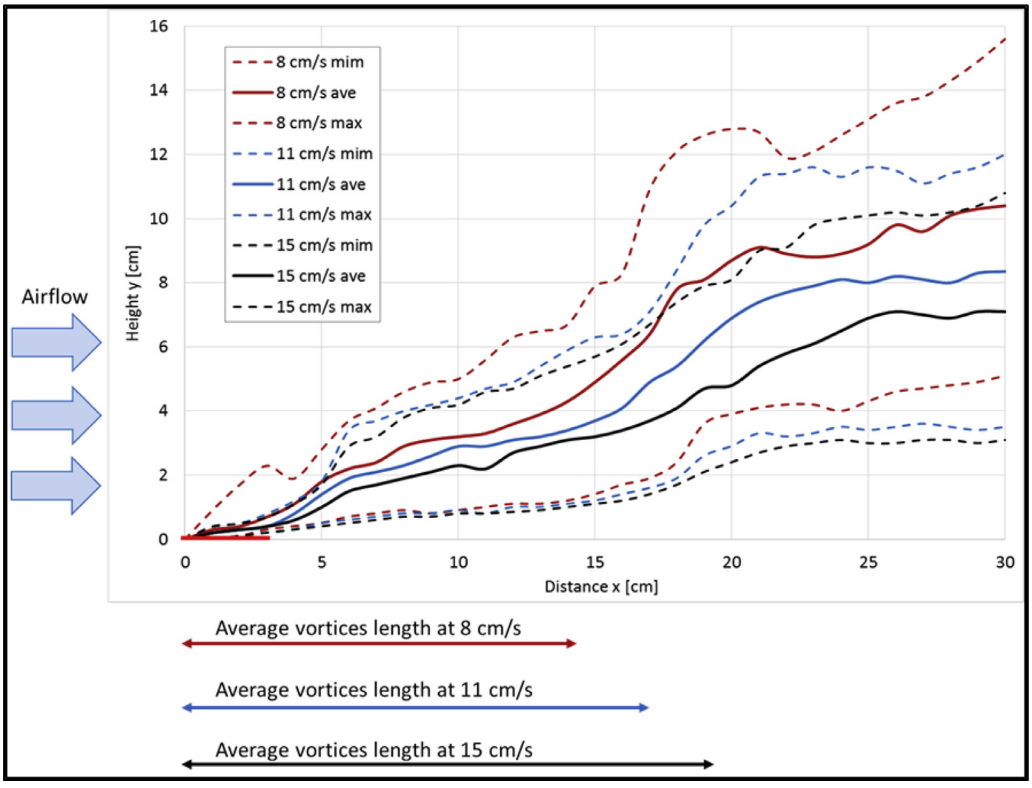

Fig. 9. Smoke streak height as a function of x and u, at $T = 200$°C.

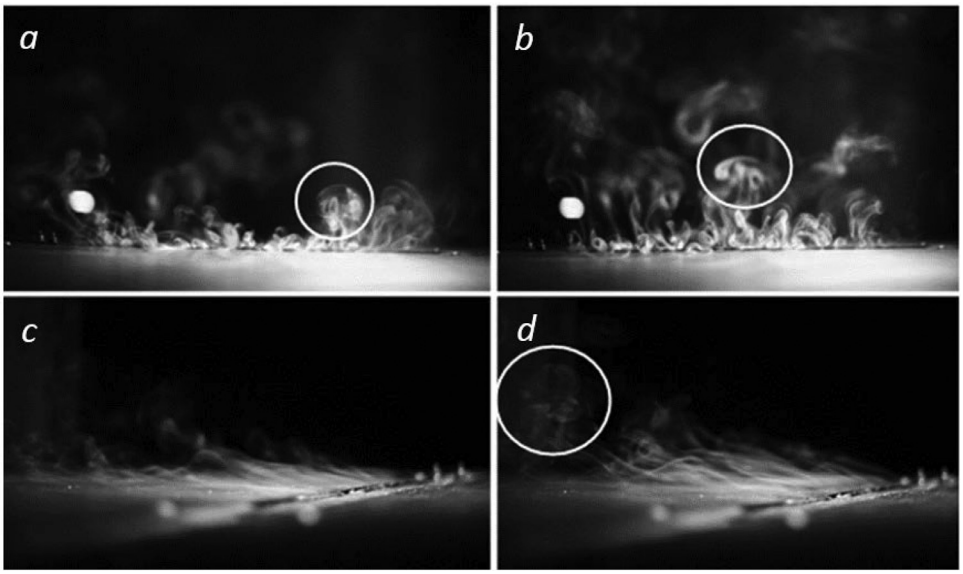

Fig. 10. Variations in smoke streak height at $u = 8$ cm/s and $T = 200$ °C; a, b – front view and c, d – side upstream view. The circled section shows mushroom shape upward motion.

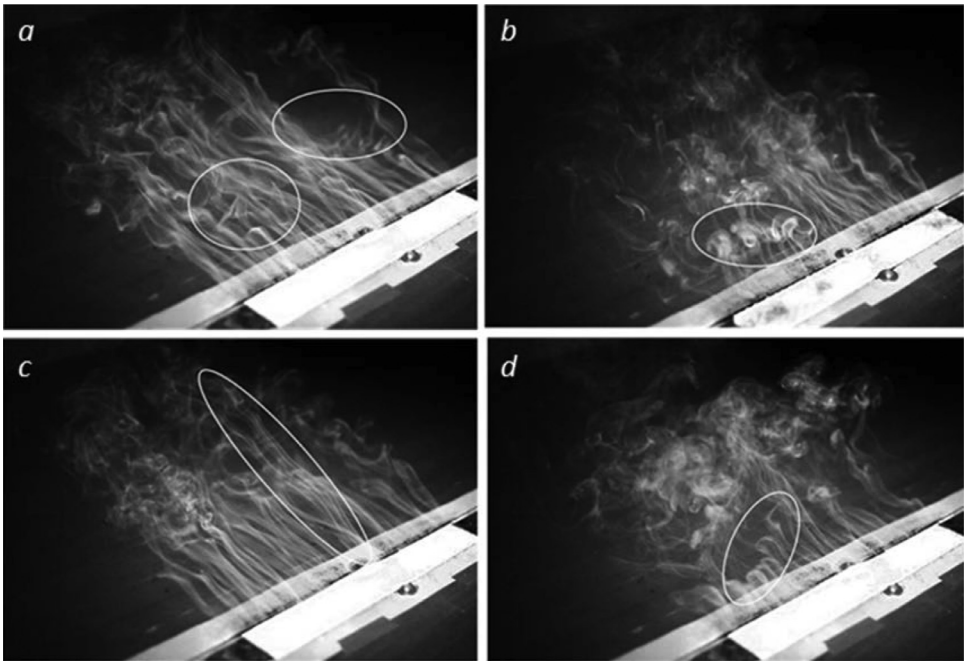

Fig. 11. Flow features of interest (circled): a – bulk rotational motion; b – upward "mushroom shape" motion; c – vortex tubes; and d – variation in vortex tubes length.

twin vortices; they eventually destabilized and would then disrupt the vortex tubes. These mushroom twin vortices seem to periodically repeat its appearance and disappearance, as shown in Fig. 11d. The appearance location of these twin vortices appeared random and helped some vortex tubes to extend longer than others (Fig. 11c).

Rotational motion of the bulk flow was also observed in the transition region between laminar-to-turbulent flow and in the turbulent regime. This rotational motion formed smoke peaks and valleys as shown in Fig. 11a. Sometimes, when this motion appeared closer to the heater, i.e., at smaller distance x, individual vortex tubes were involved, as demonstrated in Fig. 12.

We made the 2D flow visualization with the laser sheet technique for $u = 8$ cm/s, since the smoke streak structure was similar for all three different ($u = 8$, 11, and 15 cm/s) cases. We sliced the flow structure at 28 different locations within a range of $3 \le x \le 30$ cm along the x-coordinate to obtain a 2D close section image, vertical to the x coordinate. Figure 13 shows representative images of these 2D flow structures. A careful review of these images revealed that there are four different flow regimes to exist. Figure 14 depicts these four regimes.

Regime (1), $3 \le x \le 8$ cm, exhibits the well-organized flow structures consisted of several vortex tube pairs, with some tubes interacting with each other and all moving almost horizontally along the base of the test section. Regime (2), $9 \le x \le 14$ cm, the average diameter of vortex tubes increased causing greater interactions between them and generated mushroom shape twin vortices which moved upwardly. The flow direction was mostly along the x coordinate. Regime (3), $15 \le x \le 18$ cm, was characterized by a transition from organized vortex flow structures to turbulent, chaotic

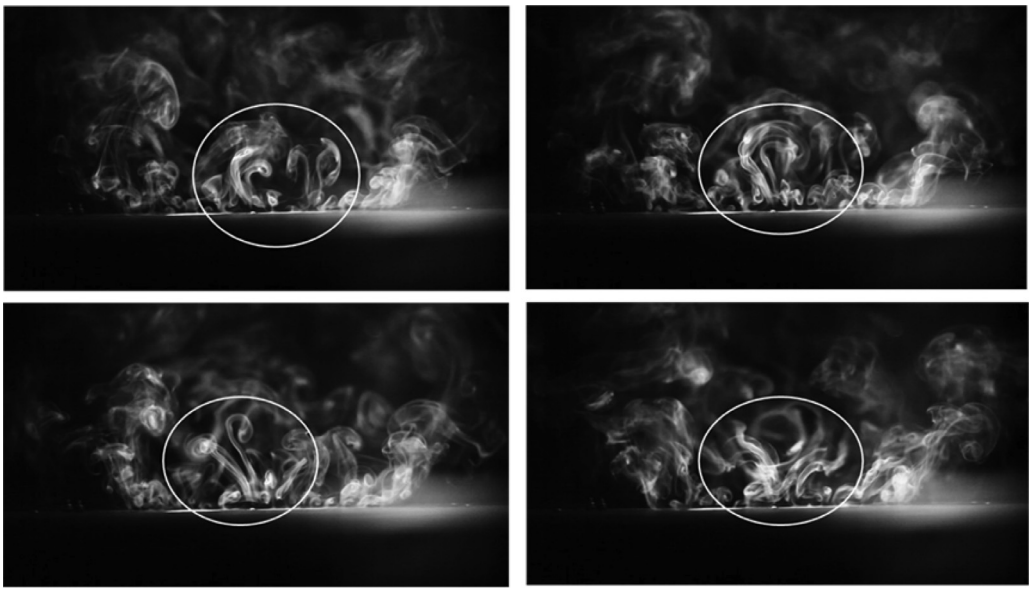

Fig. 12. Interaction between vortex tubes and bulk rotational motion (front view of approaching flow, $u = 8$ cm/s, and $T = 200$ °C).

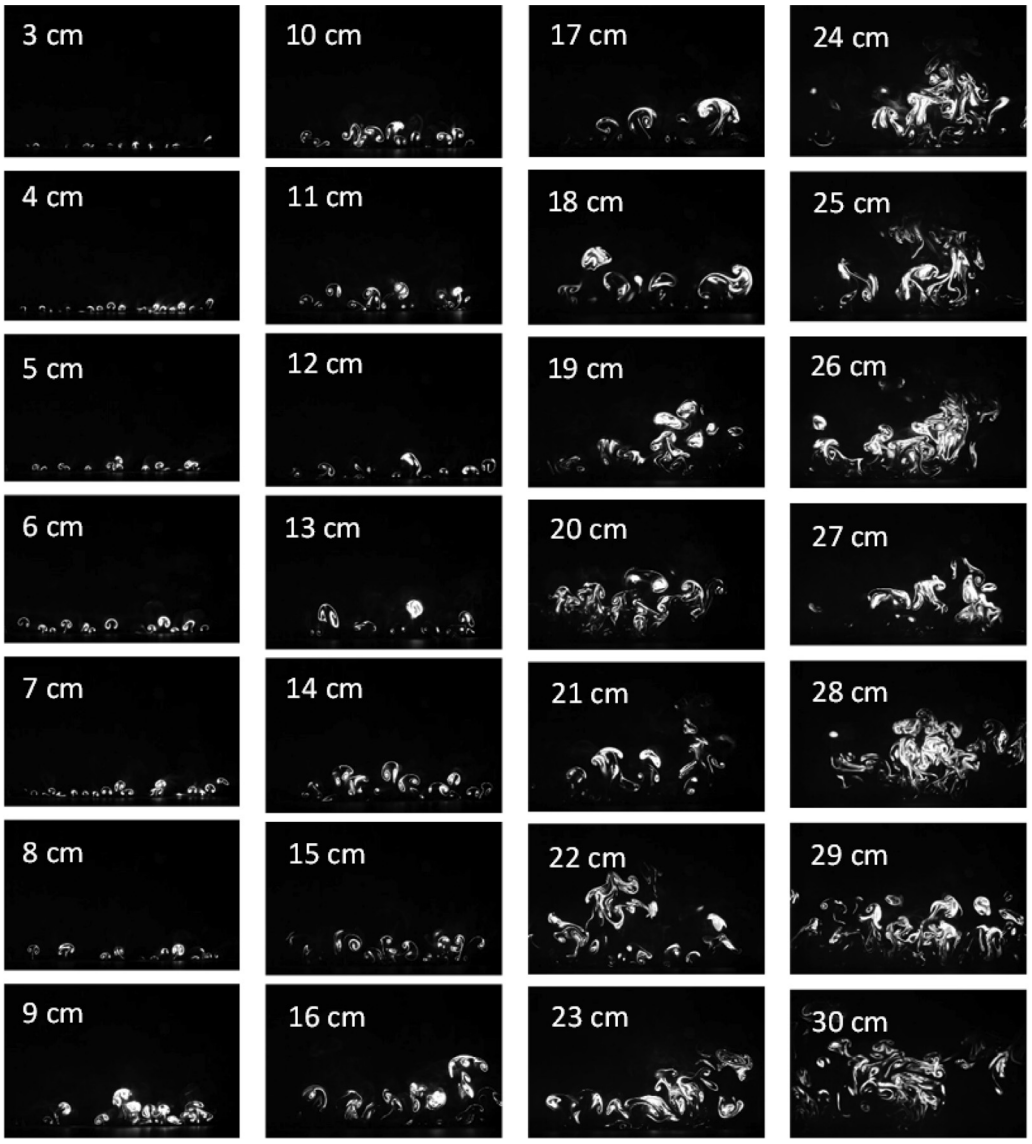

Fig. 13. A collection of images taken at 28 different laser sheet locations with $u = 8$ cm/s and $T = 200$ °C (laser illumination, front view of approaching flow).

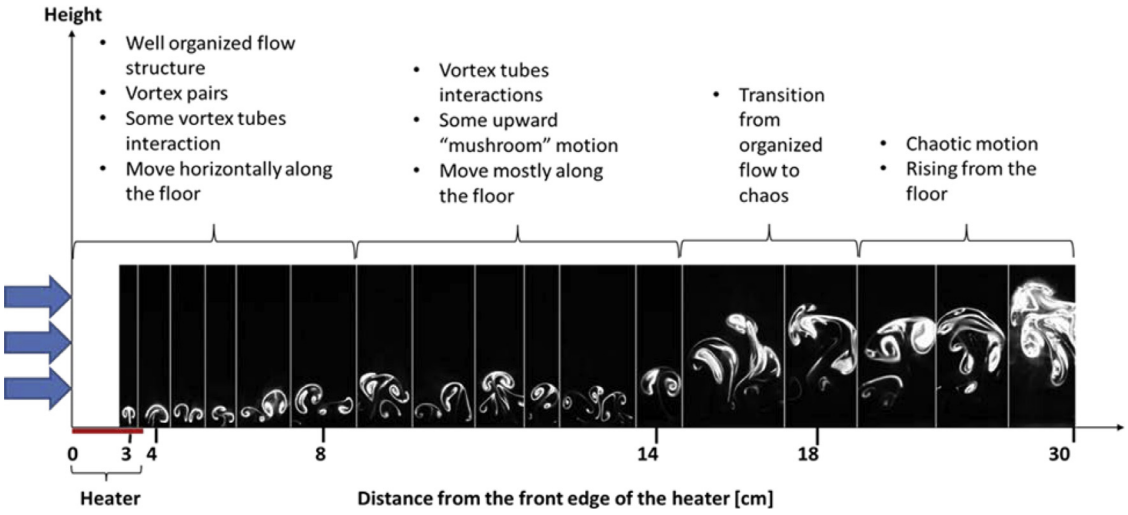

Fig. 14. Flow structures along the horizontal distance x identified from the laser sheet illumination technique ($u = 8$ cm/s and $T = 200$ °C).

flow. Regime (4), $19 \le x \le 30$ cm, included turbulent flow that was separated from the floor.

Among the above observation, a range of $3 \le x \le 14$ cm was of particular interest because the flow was horizontal along the floor and could potentially be associated with preheating length in a real fire. A close look at the results of Fig. 14 revealed that the organized flow consisting of individual vortex pairs emerged between $3 \le x \le 12$, and the average diameter of vortex tubes first increased with an increase in x, then stimulated more frequent interactions between vortices at larger distances. With $10 \le x \le 12$, the vortex tubes repulsed each other resulting in a deformed vortex shape. With $10 \le x \le 14$, some vortex pairs were above others which helped to increase the smoke streak height. Figure 16 displays some examples of interacting vortex pairs at different x locations.

5. Similarity between the current non-reactive flow experiments and the USDA'S wind tunnel fire experiments

Here we examine whether or not the current non-reactive flow visualization results are relevant to study forest fire phenomena where active combustion takes place. To that end, we compare our results to the wind tunnel fire experiments conducted at USDA Missoula Fire Science Laboratory [21].

Figure 17 shows two images from the same test within the current nonreactive smoke investigation with a difference in time of 1/15 s between the images. The rotational motion in the highlighted region led to a down-wash flow (Fig. 17b), in agreement with a down-wash motion observed by Finney et al. [22] in their fire experiments, as depicted in Fig. 18. The down-wash motion of the smoke shown in Fig. 17, therefore, is a purely hydrodynamic effect driven by convection because no fire or chemical reactions were present.

In wildland fires, flames form peaks and valley structures as a fire front propagate through the fuel bed. Additionally, the flames form mushroom shapes twin vortices with upwardly moving peaks like those shown in Fig. 19c [38] which are a leading contributor to upward fluctuations in a fire front. The same behavior may be observed during the current laboratory visualization experiments. Figure 19 compares our non-reactive flow visualization results (Fig. 19 a and b) to USDA's fire spreading experiments over cardboard fuel beds (Fig. 19c) showing a remarkable similarity between the smoke and fire behavior structure. It is a commonly accepted that fire fronts propagate in the turbulent regime for both wind tunnel and field burns [38]. This assumption can be more thoroughly examined by comparing images acquired during the current study with those obtained in mid-scale burns [38]; validation of turbulent flow propagation is seen in the mid-scale fire in regions ahead of and behind the fire front (Figs. 19c, 20b and d). However, it is not clear from these images whether this assumption holds within the fire zone.

In addition to the mushroom shape twin vortices circled in white of Fig. 19a and b from the current study, the vortex tubes circled in red highlight horizontal flow regions in the smoke which persisted until the transition region of the floor of the moving smoke where it began to rise upwards from the floor of the wind tunnel. Vortex pairs rotating in opposite directions (Fig. 20a) may well be responsible for the formation of these tubes in the flame zone, but their exact inner flow structure within the fire zone could not be imaged because of being masked by the flame itself.

Figure 15 at distances between $3 \le x \le 8$ shows behavior similar to Görtler vortices which have been observed in wind tunnel burns [22]; this Görtler behavior is represented by the well-organized flow of discrete vortex pairs moving parallel to each other. At distances larger than 8 cm from the smoke source, interactions between vortex tubes were initiated which created flow instabilities and vertical height fluctuations; this type of behavior was also detected in wind tunnel burns [22,38,60].

Despite the fact that the temperature above the heater was much higher than the surroundings, the smoke that was generated remained in almost horizontal flow and then downstream it transitioned into convective-driven, upward moving flow. That observed flow pattern can be explained by the Fr number effect. Fr number decreases as an increase in the horizontal distance from the heating source meaning that the inertial force dominates at the beginning but with an increase in the horizontal distance, the buoyancy force starts to dominate creating upward moving flow. We compared our scale model flow structure to the convection flow structure observed in the USDA's mid-scale wind tunnel fire experiments [22]. We obtained good qualitative similarity between them, as shown in Figs 19 and 20, proving the validity of our scaling laws and assumptions employed there. Our recent study [22] also proved the Fr–St scaling correlation, which is π_7 in our scaling laws, for a wide range of different scale fires.

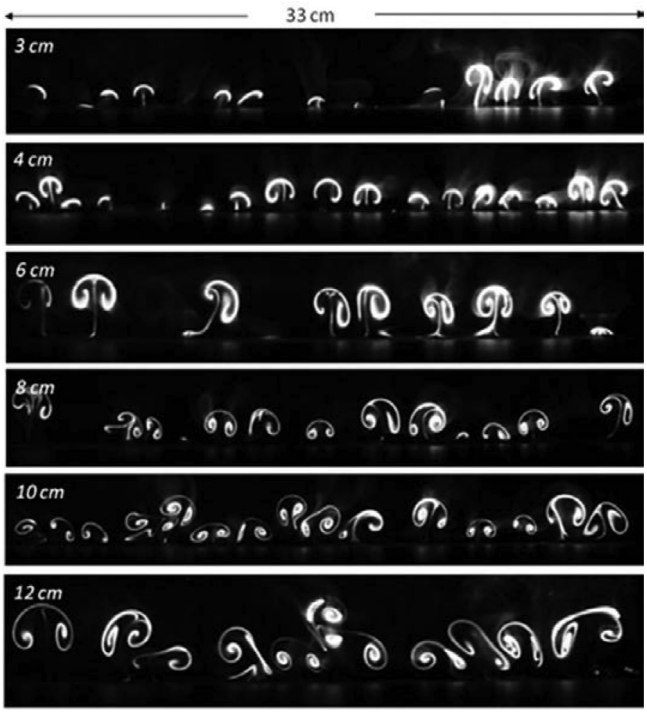

Fig. 15. Organized flow of vortex pairs.

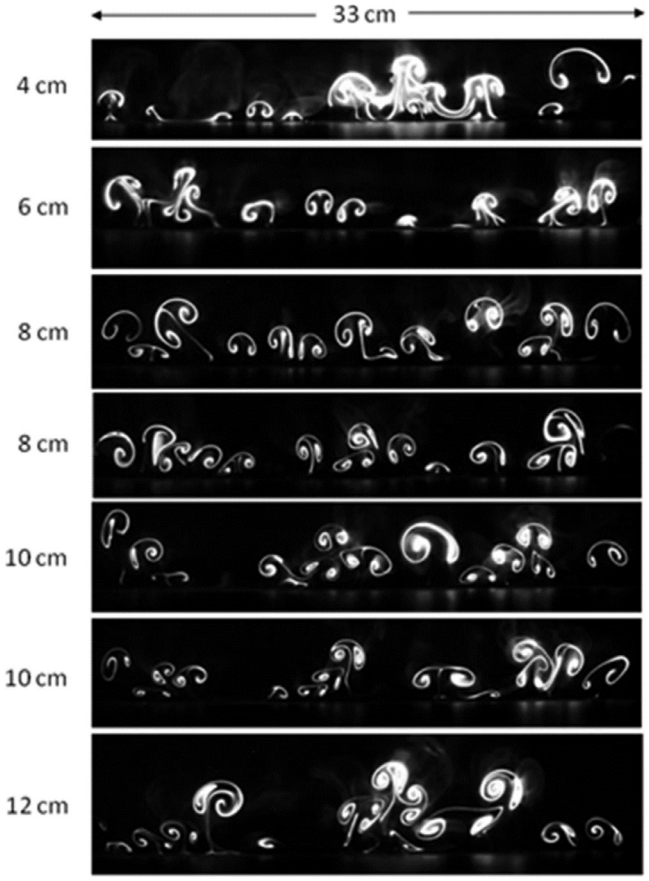

Fig. 16. Vortex pairs' interactions.

6. Scaling analysis

To assess similarity between the current non-reactive flow experimental results (called 'model' in the following discussion) and the USDA's wind tunnel fire experiments [22] (called 'full-scale' in the following), we applied the law approach technique in scale modeling [24] to estimate the magnitude of each of three Pi-numbers π_1, π_3, and π_7, identified in the scale modeling section. The calculation was made using the following relationships. Here the prime symbol represents the model and those without the symbol represent full-scale.

- $c_p = c_p$'
- $\rho_1 = \rho_1$'
- $L_a/L_a' \approx 38$, $L_a \approx 1.5$ m and $L_a' \approx 0.04$ m: L_a was approximated by examining previously published data [22]. L_a' was the height estimated by using IR camera imaging and represented the distance above the heater, where the IR determined plume temperature dropped to roughly 50 °C from 200 °C at the tip of smoke column [61].
- $R/R' \approx 13$, where at full-scale $R \approx 1$ m/s [24] whereas for the model R' = 0.08 m/s.
- $\Delta\theta/\Delta\theta' \approx 1000/200 = 5.0$.
- $l_2/l_2' \approx 2/0.33 \approx 6$, where full-scale l_2 was from previously published data [21,24,38] and the model $l_2' = 0.33$ m.
- $L_w/L_w' \approx 1/0.035 \approx 29$, where full-scale L_w was taken from previously published data [21,24,38] and the model $L_w' = 0.035$ m.
- $L_e/L_e' \approx 1/0.02 \approx 50$, where full-scale L_e was taken from previously published data [24,38] and $L_e' = 0.02$ m was estimated by using images from an IR camera.
- $u/u' = 1/0.08 \approx 13$.
- $w/w' = 0.5/2 = 0.25$, where full-scale w was based on previously published data [38] and w' was approximated from the model visualization results.
- $I/I' = 25/0.08 \approx 31$, where the full-scale value of I was from previously published data [38] and model value is $I' = 2\ \mathrm{kW/m^2} * 0.04\ \mathrm{m} = 0.08\ \mathrm{kW/m}$.

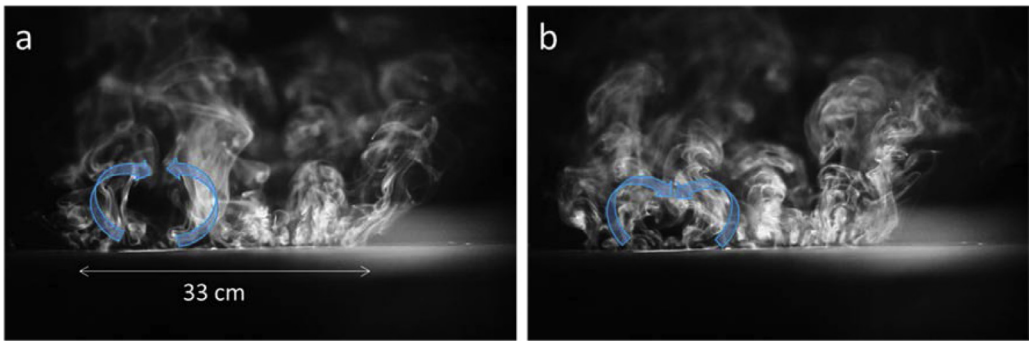

Fig. 17. Time evolution of rotational flow within the transition region: a – 0 s; b – 1/15 s (front view of approaching flow, $u = 8$ cm/s and $T = 200$ °C).

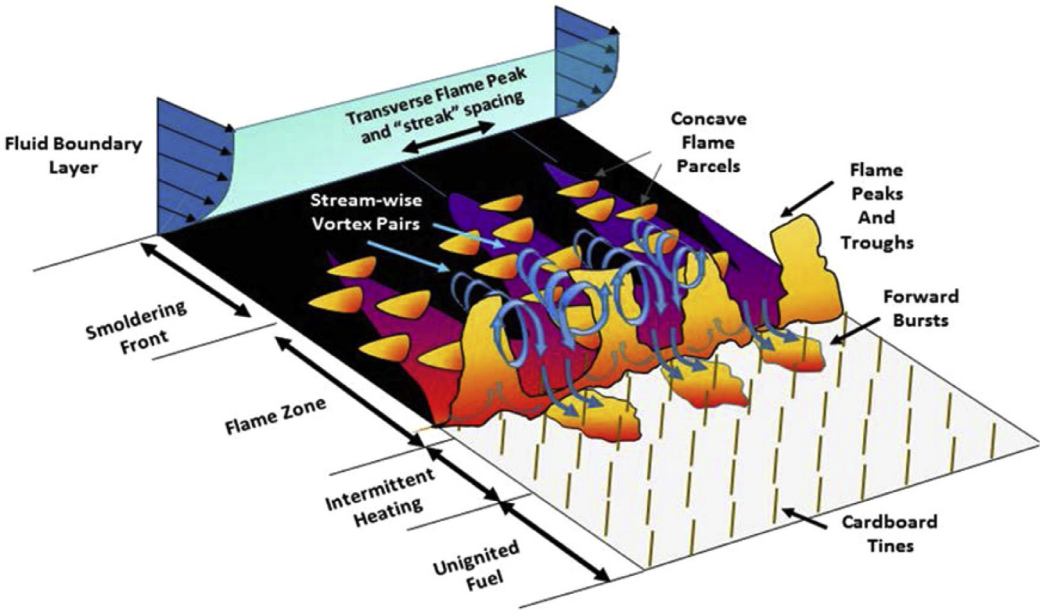

Fig. 18. Schematic representation of flame propagating through a cardboard fuel bed [22] showing the down-wash motion that was associated with the flame spread.

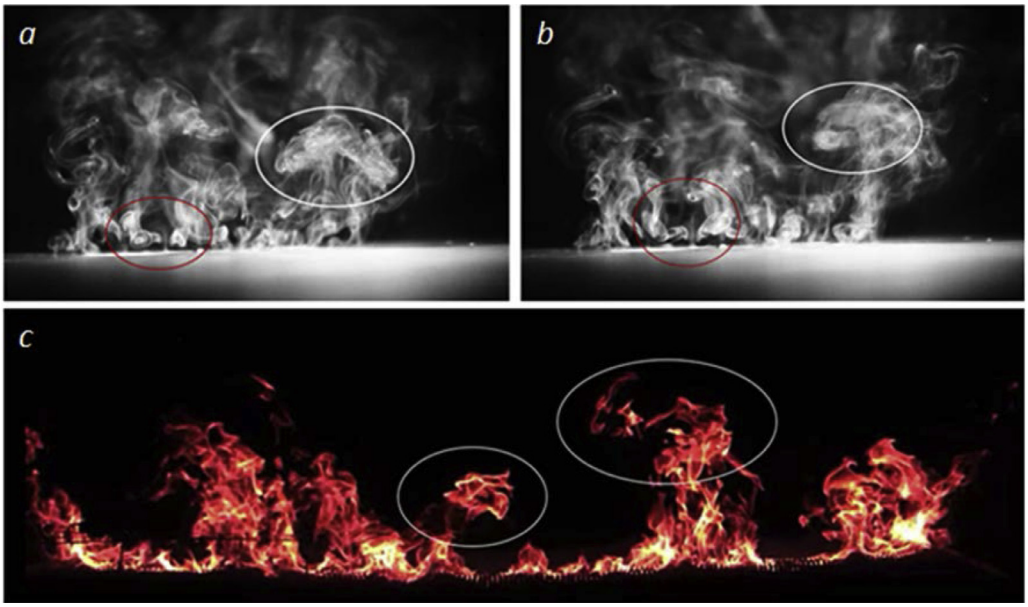

Fig. 19. Comparison between the non-reactive flow behavior (a and b, current study) and the wind tunnel fire spreading test (c) [38]. Circled areas (white) show the structural similarity of plume created by the non-reactive flow and the wind tunnel fire. (For interpretation of the references to color in this figure, the reader is referred to the web version of this article.)

The scaling resulted in the following relations:

$$\pi_1 = k_1{}^{*}\pi_1{}'k_1 \approx 1; \pi_2 = k_2{}^{*}\pi_2{}'k_2 \approx 1; \pi_4 = k_4{}^{*}\pi_4{}'k_4 \approx 2.$$

where: k_1, k_2, and k_3 were the scaling constants, which can be determined from the scaling ratio between the full scale and the corresponding scale model [24].

The above results confirm that the same physical laws governed both model and full-scale and satisfy the similarity criteria established by the law approach [24,56]. This is interesting since the full scale is fire experiments where active combustion takes place, while the scale model is non-reactive flow experiments, mostly focusing on convective heat transfer aspects. However, it may not be so surprising, because we previously reconstructed a moving type fire whirl only using heated narrow wire tapes and wind tunnel [25] using the Fr number scaling. So our current success seems to suggest that different aspects of forest and wildland fire phenomena can be simulated by simple nonreactive flow and heat transfer experiments.

7. Conclusions

(1) Flow visualization and imaging using nonreactive smoke generation and flow experiments revealed detailed flow structures that were created by interactions of heater-generated upward flow and horizontal airflow within a small wind tunnel. The four flow structures identified included: (1) organized horizontal vortex flows, (2) weak vortex flow interactions, (3) strong vortex flow interactions, and (4) turbulent flows. It was found

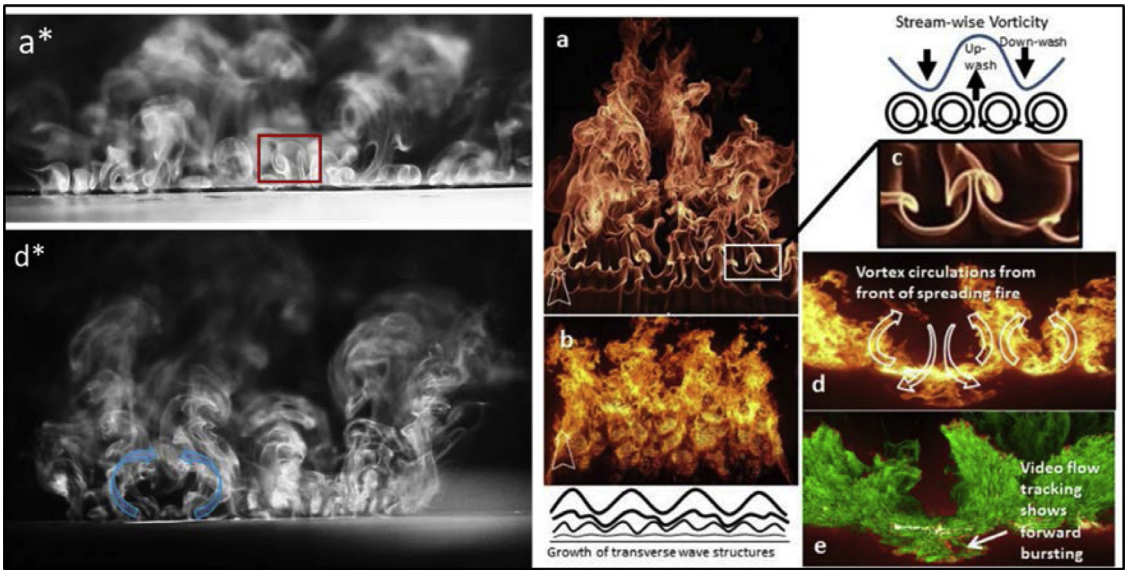

Fig. 20. Comparison between non-reactive flow behavior (shown in the left column indicated as **a*** and **d***) and the USDA' wind tunnel burns [22] (shown in the right two columns indicated as **a** through **e**). The non-reactive photograph a* is similar to the corresponding wind tunnel burn photograph **a**, and the non-reactive photograph **d*** is similar to the corresponding wind tunnel burn photograph **d**. The non-reactive photographs in Fig. 7 are similar to **c**.

that the height of the smoke above the floor of the wind tunnel increased with an increase in the horizontal distance x and decreased with an increase in the horizontal airflow velocity, u.

(2) We conducted scaling analysis to assess the similarity between the current non-reactive scale-model flow structure to the full-scale burns. As a result, three key Pi-numbers, including the Fr number, the St number, and $\pi_3 = Qc/Q$, were shown to be identical for the full scale and the corresponding scale model experiments, thereby satisfying similarity between both experiments.

(3) The present (nonreactive flow) experimental study was relevant to simulate the fluid dynamics structure of fire behavior. It allows detailed imaging of the flow field in and around the fire-zone as well as the application of scaling laws [3,19,38] at variable temperatures and heat fluxes. An experimental setup with a flat heated plate can be used to simulate the area behind (upstream) a fire zone where burnt products are still hot enough to generate enough buoyancy (left side of Fig. 1) which then interacts with horizontal airflow (driven by inertia) and creates vortex flow. Thus, the fire zone may experience upcoming well-organized vortex flow rather than chaotic turbulent (wildfire case) or laminar (wind tunnel burns) one.

(4) Haines and Smith [41–43] applied low speed airflow parallel to the heat wire which represents fire generated heat and succeeded in recreating vortex pairs above the wire. They suggested Gr number and Ra number for scaling without specifically validating the role of each of these pi-numbers, to help connect their laboratory observations to the full-scale fires. This study's major contribution is that we applied our scaling laws [3] to design the current laboratory-scale flow visualization experiments and found that the observed vortices were similar to the vortices observed in the USDA's mid-scale wind tunnel fire spreading experiments [22], therefore validating the above scaling laws and assumptions employed there. Interestingly, despite different flow orientation relative to the heater, both Haines and Smith [41–43] and the current study found very similar shape vortices, indicating that their horizontal vortices might well be formed in our experiments, which is a scaled-down version of the USDA's fire spreading experiments [22]. This seemingly coincidental finding suggests the need for further study whether or not the horizontal vortices and the USDA's convection-driven fire spreading model [22] is related each other.

Acknowledgment

This study was sponsored by a grant (17-CS-11221637-099) from USDA Forest Service, Missoula, MT. We also acknowledge that the current work is a continuation of a long history of work performed by USDA Forest Service scientists and collaborators and part of a larger national effort to better understand wildland fires which is focused within the research branch of the USDA Forest Service.

References

[1] G.M. Byram, Forest fire behavior, in: K.P. Davis (Ed.), Forest fire: control and use, 1st ed., McGraw-Hill, New York, NY, 1959, pp. 89–123.
[2] G.M. Byram, H.B. Clements, M.E. Bishop, R.M.J. Nelson, Project fire model – an experimental study of model fires, USDA Forest Service, Southeastern Forest and Range Experiment Station, Macon, GA, 1966 http://www.treesearch.fs.fed.us/pubs/45219.
[3] R.I. Emori, K. Saito, A study of scaling laws in pool and crib fires, Combust. Sci. Technol. 31 (1983) 217–230.
[4] R.M. Nelson Jr., Power of the fire-a thermodynamic analysis, Int. J. Wildland Fire 12 (2003) 51–65.
[5] M. Finney, J. Cohen, S. McAllister, W. Jolly, On the need for a theory of wildland fire spread, Int. J. Wildland Fire 22 (2013) 25–36.
[6] M. Grishin, V. Zima, V. Kuznetsov, A. Skorik, Ignition of combustible forest materials by radiant heat flux, Combust. Explos. Shock Waves 38 (2002) 24–29.
[7] P. Mindykowski, A. Fuentes, J. Consalvi, B. Porterie, Piloted ignition of wildland fuels, Fire Saf. J. 46 (2011) 34–40.
[8] W.L. Fons, Analytical considerations of model forest fire, University of California, 1940 M.S.
[9] W.L. Fons, Analysis of fire spread in light forest fuels, J. Agric. Res. 72 (1946) 92–121.
[10] R.J. McCarter, A. Broido, Radiative and convective energy from wood crib fires, Pyrodynamics 2 (1965) 65–85.
[11] R.J. McCarter, A. Broido, A calorimeter for determining radiation and convection in small-scale combustions, Pyrodynamics 4 (1966) 191–203.
[12] S. Scesa, Transfer of heat by forced convection from a line combustion source-the influence of atmospheric stability and surface roughness, USDA Forest Service, Division of Fire Research, Washington, D.C., 1957 Interim Technical Report AFSWP-865.
[13] S. Scesa, F.M. Sauer, Possible effects of free convection on fire behavior – Laminar and turbulent line and point sources of heat, USDA Forest Service, California Forest and Range Experiment Station, Berkeley, CA, 1954 https://www.fs.usda.gov/treesearch/pubs/55806.

[14] H.E. Anderson, Heat transfer and fire spread, USDA Forest Service, Intermountain Forest & Range Experiment Station, Ogden, UT, 1969 http://www.treesearch.fs.fed.us/pubs/40489.
[15] P.J. Pagni, T.G. Peterson, Flame spread through porous fuels, Symp. (Int.) Combust. 14 (1973) 1099–1107.
[16] F.A. Albini, A model for fire spread in wildland fuels by-radiation, Combust. Sci. Technol. 42 (1985) 229–258.
[17] H. Telisin, Flame radiation as a mechanism of fire spread in forests, in: N. Afgan, J. Beer (Eds.), Heat Transfer in Flames, John Wiley, New York, 1974, pp. 441–449.
[18] B.W. Butler, J. Cohen, D.J. Latham, R.D. Schuette, P. Sopko, K.S. Shannon, D. Jimenez, L.S. Bradshaw, Measurements of radiant emissive power and temperatures in crown fires, Canadian J. Forest Res. 34 (2004) 1577–1587.
[19] R.I. Emori, Y. Iguchi, K. Saito, I.S. Wichman, Simplified scale modeling of turbulent flame spread with implication to wildland fires, Fire Saf. Sci. 2 (1989) 263–273.
[20] H.C. Hottel, Fire modeling, International Symposium on the Use of Models in Fire Research, National Academy of Sciences, National Research Council, Washington, DC (1961).
[21] B.A. Adam, N.K. Akafuah, M. Finney, J. Forthofer, K. Saito, A study of flame spread in engineered cardboard fuelbeds. Part II: scaling law approach, in: K. Saito, A. Ito, Y. Nakamura, K. Kuwana (Eds.), Progress in Scale Modeling, 2, Springer, Cham, Switzerland, 2014, pp. 85–95.
[22] M.A. Finney, J.D. Cohen, J.M. Forthofer, S.S. McAllister, M.J. Gollner, D.J. Gorham, K. Saito, N.K. Akafuah, B.A. Adam, J.D. English, The role of buoyant flame dynamics in wildfire spread, Proc. Natl. Acad. Sci. 112 (2015) 9833–9838.
[23] D. Frankman, B.W. Webb, B.W. Butler, D. Jimenez, J.M. Forthofer, P. Sopko, K.S. Shannon, J.K. Hiers, R.D. Ottmar, Measurements of convective and radiative heating in wildland fires, Int. J. Wildland Fire 22 (2014) 157–167.
[24] R.I. Emori, K. Saito, K. Sekimoto, Scale models in engineering (mokei jikken no riron to ohyou), Third ed., Gihodo Publishing Co., Tokyo, Japan, 2000 in Japanese.
[25] D. Tillman, A. Rossi, W. Kitto, Wood combustion: principles, processes and economics, Academic Press, New York, 1981.
[26] B.M. Cetegen, Y. Dong, Experiments on the instability modes of buoyant diffusion flames and effects of ambient atmosphere on the instabilities, Exp. Fluids 28 (2000) 546–558.
[27] X. Jiang, K.H. Luo, Dynamics and structure of transitional buoyant jet diffusion flames with side-wall effects, Combust. Flame 133 (2003) 29–45.
[28] H. Gotoda, Y. Asano, K.H. Chuah, G. Kushida, Nonlinear analysis on dynamic behavior of buoyancy-induced flame oscillation under swirling flow, Int. J. Heat Mass Transf. 52 (2009) 5423–5432.
[29] R.M. Banta, L.D. Olivier, E.T. Holloway, R.A. Kropfli, B.W. Bartram, R.E. Cupp, M.J. Post, Smoke-column observations from two forest fires using Doppler lidar and Doppler radar, J. Appl. Meteor. 31 (1992) 1328–1349.
[30] T.L Clark, L. Radke, J. Coen, D. Middleton, Analysis of small-scale convective dynamics in a crown fire using infrared video camera imagery, J. Appl. Meteor. 38 (1999) 1401–1420.
[31] J. Coen, S. Mahalingam, J. Daily, Infrared imagery of crown-fire dynamics during FROSTFIRE, J. Appl. Meteor. 43 (2004) 1241–1259.
[32] A. Bejan, Plumes, Convection Heat Transfer, third ed., John Wiley & Sons, Inc, Hoboken, New Jersey, 2004, pp. 430–439.
[33] V. Kottke, Taylor–Görtler vortices and their effect on heat and mass transfer, 8th International Heat Transfer Conference, San Francisco, CA (1986).
[34] P.D. McCormack, H. Welker, M. Kelleher, Taylor-Görtler vortices and their effect on heat transfer, J. Heat Transf. 92 (1970) 101–112.
[35] J. Lozano, W. Tachajapong, H. Pan, A. Swanson, C. Kelley, M. Princevac, S. Mahalingam, Experimental investigation of the velocity field in a controlled wind-aided propagating fire using particle image velocimetry, Fire Saf. Sci. 9 (2008) 255–266.
[36] J. Lozano, An investigation of surface and crown fire dynamics in shrub fuels, University of California, 2011.
[37] J. Lozano, W. Tachajapong, D.R. Weise, S. Mahalingam, M. Princevac, Fluid dynamic structures in a fire environment observed in laboratory-scale experiments, Combust. Sci. Technol. 182 (2010) 858–878.
[38] B.A. Adam, Incorporating dynamic flame behavior into the scaling laws of wildland fire spread, 2015.
[39] F.A. Williams, Scaling mass fires, Fire Res. Abstr. Rev. 11 (1969) 1–23.
[40] R.I. Emori, K. Saito, Model experiment of hazardous forest fire whirl, Fire Technol. 18 (1982) 319–327.
[41] D.A. Haines, M.C. Smith, Simulation of the collapse of bent-over vortex pairs observed in wildland fires, Forest Sci. 38 (1992) 68–79.
[42] D.A. Haines, M.C. Smith, Wind tunnel generation of horizontal roll vortices over a differentially heated surface, Nature 306 (1983) 351–352.
[43] D.A. Haines, M.C. Smith, Three types of horizontal vortices observed in wildland mass and crown fires, J. Climate Appl. Meteor. 26 (1987) 1624–1637.
[44] D.A. Haines, Horizontal roll vortices and crown fires, J. Appl. Meteor. 21 (1982) 751–763.
[45] F.A. Williams, Mechanism of flame spread, Symp. (Int.) Combust. 16 (1976) 1281–1292.
[46] D.B. Spalding, Colloquium on modeling principles: the art of partial modeling, Symp. (Int.) Combust. 9 (1963) 833–843.
[47] K. Saito, F.A. Williams, Scale modeling in the age of high-speed computation, in: K. Saito, A. Ito, Y. Nakamura, K. Kuwana (Eds.), Progress in Scale Modeling, 2, Springer, Cham, Switzerland, 2014, pp. 1–18.
[48] H.W. Emmons, T. Shen, Fire spread in paper arrays, Symp. (Int.) Combust. 13 (1971) 917–926.
[49] H.W. Emmons, Some observations on pool burning, International Symposium on the Use of Models in Fire Research, National Academy of Sciences-National Research Council, Washington (1961), pp. 50–67.
[50] F.E. Fendell, M.F. Wolff, Wind-aided fire spread, in: E. Johnson, K. Miyanishi (Eds.), Forest Fires: Behavior and Ecological Effects, Academic Press, San Diego, 2001, pp. 171–224.
[51] G. Heskestad, Virtual origins of fire plumes, Fire Saf. J. 5 (1983) 109–114.
[52] S.W. Taylor, B.M. Wotton, M.E. Alexander, G.N. Dalrymple, Variation in wind and crown fire behavior in a northern jack pine black spruce forest, Ca. J. For. Res. 34 (2004) 1561–1576.
[53] R. Raupach, J.J. Finnigan, Y. Brunei, Coherent eddies and turbulence in vegetation canopies: the mixing-layer analogy, Boundary-Layer Meteorol. 78 (1996) 351–382.
[54] C.B. Clements, B.E. Potter, S. Zhong, In situ measurements of water vapor, heat, and CO_2 fluxes within a prescribed grass fire, Int. J. Wildland Fire 15 (2006) 299–306.
[55] R.O. Weber, Modelling fire spread through fuel beds, Prog. Energy Combust. Sci. 17 (1991) 67–82.
[56] K. Saito, N.K. Akafuah, Scaling, in: S.L. Manzello (Ed.), Encyclopedia of wild fires and wildland –urban interface (WUI) fires, Springer, Cham, Switzerland, 2018.
[57] M.A. Finney, J.D. Cohen, J.A. Forthofer, S.S. McAllister, B.A. Adam, N.K. Akafuah, J. English, K. Saito, D.J. Gorham, M.J. Gollner, Experimental evidence of buoyancy controlled flame spread in wildland fires, Advances in Forest Fire Research, Coimbra (2014).
[58] P. Cunningham, R.R. Linn, Numerical simulations of grass fires using a coupled atmosphere-fire model: dynamics of fire spread, J. Geophys. Res. Atmos. 112 (2007) 1–17.
[59] J.D. Cohen, M.A. Finney, Fine fuel particle heating during experimental laboratory fires, Advances in Forest Fire Research, Coimbra (2014).
[60] D.J. Gorham, M.J. Gollner, Buoyant instabilities in steady and propagating flames, 8th US National Combustion Meeting, University of Utah (2013) May 19–22.
[61] A. Arakawa, K. Saito, W.A. Gruver, Automated infrared imaging temperature measurement: with application to upward flame spread studies, Combust. Flame 92 (1993) 222–230.